

# The extremely asymmetric radio structure of the $z=3.1$ radio galaxy B3 J2330+3927

M-A. Pérez-Torres<sup>1</sup> and C. De Breuck<sup>2</sup>

<sup>1</sup>*Instituto de Astrofísica de Andalucía, CSIC, Apdo. Correos 3004, E-18080 Granada, Spain*

<sup>2</sup>*European Southern Observatory, Karl Schwarzschild Straße 2, D-85748 Garching, Germany*

Accepted 2005 July 15. Received 2005 July 14; in original form 2005 June 29.

## ABSTRACT

We report on 1.7 and 5.0 GHz observations of the  $z = 3.087$  radio galaxy B3 J2330+3927, using the Very Long Baseline Array (VLBA), and archival 1.4 and 8.4 GHz Very Large Array (VLA) data. Our VLBA data identify a compact, flat spectrum ( $\alpha_{1.7 \text{ GHz}}^{5 \text{ GHz}} = -0.2 \pm 0.1$ ;  $S_\nu \propto \nu^\alpha$ ) radio component as the core. The VLA images show that the fraction of core emission is very large ( $f_c \approx 0.5$  at 8.4 GHz), and reveal a previously undetected, very faint counterjet, implying a radio lobe flux density ratio  $R \gtrsim 11$  and a radio lobe distance ratio  $Q \approx 1.9$ . Those values are much more common in quasars than in radio galaxies, but the optical/near-IR spectra show a clear type II AGN for B3 J2330+3927, confirming that it is indeed a radio galaxy. Unlike all other radio galaxies, the bright Ly- $\alpha$  emitting gas is located towards the furthest radio arm. We argue against environmental and relativistic beaming effects being the cause of the observed asymmetry, and suggest this source has intrinsically asymmetric radio jets. If this is the case, B3 J2330+3927 is the first example of such a source at high redshift, and seems to be difficult to reconcile with the unified model, which explains the differences between quasars and radio galaxies as being due to orientation effects.

**Key words:** galaxies: high redshift – galaxies: jets – galaxies: individual (B3 J2330+3927)

## 1 INTRODUCTION

High redshift radio galaxies (HzRGs,  $z > 2$ ) are excellent probes to explore massive galaxies and their proto-cluster environments in the early Universe (e.g., De Breuck et al. 2002; Rocca-Volmerange et al. 2004; Venemans et al. 2004). HzRGs are also ideal tools for probing the activity of AGN in their host galaxies. Indeed, the powerful jets and ionizing radiation from young radio AGN can dramatically affect the environment of their forming host galaxies. This is clearly illustrated by the “alignment effect” of optical line-emission and UV-continuum along the radio jets (e.g., Chambers 1987; McCarthy et al. 1991), and recent discoveries of similarly radio/X-ray aligned emission (e.g., Carilli et al. 2002, Scharf et al. 2003, Overzier et al. 2005). Collimated radiation from the AGN may scatter off surrounding material, while the jets shock and heat the ambient gas and may even trigger star formation (e.g., Bicknell et al. 2000). Thus HzRGs may affect, at least temporarily, the evolution of their hosts.

High-resolution radio imaging of HzRGs, especially if combined with high-resolution optical and X-ray studies, is

essential to make progress on some of the above issues. In particular, morphological comparisons of radio and optical continuum images may help identify effects of jet-induced star formation. Similarly, comparisons of high-resolution radio and Ly- $\alpha$  images may point to the interaction between the propagating jet and the surrounding primeval interstellar medium. The importance of such environmental effects is well established by the correlated radio and optical asymmetries in powerful radio sources (McCarthy et al. 1991).

Radio galaxies at high redshifts are inevitably younger, and have smaller angular sizes than their lower redshift counterparts (Blundell & Rawlings 1999). In many cases, their central structures are much smaller than  $1''$ , and cannot be resolved even with the VLA in A-array. Very-long-baseline interferometry (VLBI) is therefore needed to resolve the central components and identify their radio cores. The milliarcsecond (mas) resolution obtained with VLBI also allows us to morphologically identify the radio cores, and to study the radio jet structures.

In this *Letter*, we present high-resolution imaging of the HzRG B3 J2330+3927 (4–11 mas resolution), obtained with the VLBA at 1.7 and 5 GHz. We also present archival 1.4 and

8.4 GHz data from the VLA. Our VLBA observations clearly identify the radio core with a compact, flat spectrum source, coincident with the optical/near-IR AGN emission and the peak of the CO emission. The deep 1.4 GHz VLA image shows a very weak counterjet, implying that B3 J2330+3927 has one of the most asymmetric radio structures ever reported for a type II AGN. We assume a  $\Lambda$ -dominated universe with  $\Omega_M = 0.3$ ,  $\Omega_\Lambda = 0.7$ , and  $H_0 = 65 \text{ km s}^{-1} \text{ Mpc}^{-1}$ . At  $z = 3.087$ ,  $1''$  corresponds to 8.2 kpc.

## 2 THE HIGH-REDSHIFT RADIO GALAXY B3 J2330+3927

The radio galaxy B3 J2330+3927 has been comprehensively studied at several frequencies by De Breuck et al. (2003), hereafter DB03. The 8.4 GHz VLA observations of DB03 showed that B3 J2330+3927 is a  $\sim 2''$  wide source consisting of three radio components, located in between two optical ( $K$ -band) objects (*a* and *b*; see Fig. 2 of DB03). Based on its radio morphology, DB03 suggested that the marginally resolved central component might be the radio core. However, optical and near-IR Keck spectroscopy of object *a* showed that B3 J2330+3927 has a classical AGN type II spectrum at  $z = 3.087$ , suggesting that this object hosts the radio core. If this is the case, a very peculiar one-sided jet morphology was then implied for B3 J2330+3927.

The 113 GHz observations of DB03 with the IRAM Plateau de Bure Interferometer revealed CO  $J=4-3$  emission peaking at a position coincident with component *a*, and at a velocity that closely corresponded to the velocity shift of an associated H I absorber seen in Ly- $\alpha$ . This strongly suggested that both CO emission and H I absorption originated from the same gas reservoir surrounding the host galaxy. DB03 estimated a molecular hydrogen mass  $M(\text{H}_2) = 7 \times 10^{10} \text{ M}_\odot$ , indicating that the host galaxy must be surrounded by a massive gas reservoir.

## 3 RADIO OBSERVATIONS OF B3 J2330+3927

### 3.1 VLA observations

We reanalyzed the 8.4 GHz observations of B3 J2330+3927 (DB03) made on 2002 March 30 with the VLA in A-configuration. The observations were made in standard continuum mode, using a bandwidth of 50 MHz. We used a scan on 3C 48 from the previous observations to set the absolute VLA flux density scale. The compact source J2257+4154 was used as the phase calibrator. We used standard amplitude calibration and phase self-calibration techniques within *AIPS* to obtain the 8.4 GHz VLA image of B3 J2330+3927 in Fig. 1. The total cleaned flux density in the image is  $\approx 21.4 \text{ mJy}$  and the image off-source rms  $\sim 40 \mu\text{Jy}/\text{beam}$ .

We also analyzed archival 1.4 GHz data obtained with the VLA in A-configuration on 20 January 2001, kindly provided by R. Ivison. The observations were done in pseudo-continuum, spectral line mode with  $7 \times 3.125$  MHz bandwidth and a central frequency of 1.400 GHz. We imaged B3 J2330+3927 using uniform weighting, resulting in a synthesized beam size of  $1''.00 \times 0''.95$ . The total cleaned flux density in the image is  $\approx 104.3 \text{ mJy}$  and the image off-source rms  $\sim 60 \mu\text{Jy}/\text{beam}$ .

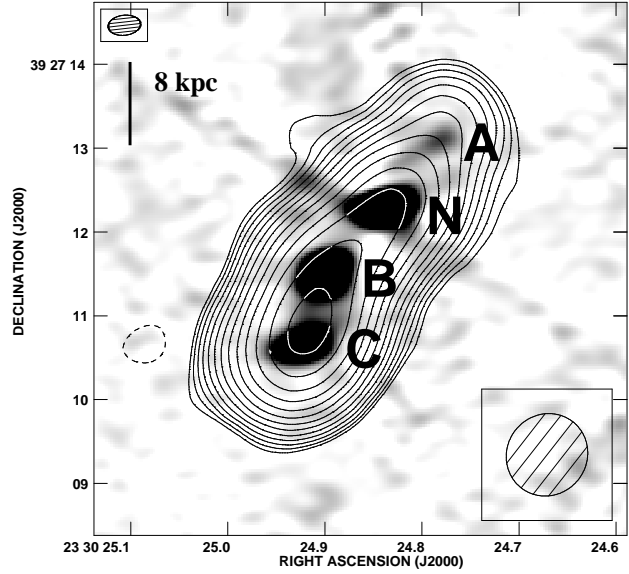


**Figure 1.** VLA A-array images of B3 J2330+3927. Greyscales show the naturally weighted 8.4 GHz image, and contours the uniformly weighted 1.4 GHz image. The contour scheme is a geometric progression in  $\sqrt{2}$ . The first contour level is at  $0.6 \text{ mJy beam}^{-1}$ . The synthesized beams are shown in the top left (8.4 GHz) and bottom right (1.4 GHz) corners. Note the confirmation of the weak 8.4 GHz component A by the 1.4 GHz contours.

### 3.2 VLBA observations

We observed B3 J2330+3927 on 2004 November 29 and December 9 with the VLBA at 1.7 and 5 GHz, respectively. We observed at a bit rate of 128 Mbit/s, and each frequency band was split into four intermediate frequencies (IFs) of 8 MHz bandwidth each, for a total synthesized bandwidth of 32 MHz. Each IF was in turn split into 32 channels of 0.25 MHz bandwidth each. The data were correlated at the VLBA Correlator of the National Radio Astronomy Observatory (NRAO) in Socorro, using an averaging time of 2 s.

Our target source, B3 J2330+3927, was observed in phase-reference mode. B3 J2330+3927 and the nearby ( $\sim 40''$ ), International Celestial Reference Frame (ICRF) source J2333+3901 were alternately observed through each six-hour long VLBA run. The observations consisted of  $\sim 180$  s scans on B3 J2330+3927 and  $\sim 100$  s scans on J2333+3901, plus  $\sim 20$  s of antenna slew time. In each observing run, the total on-target time was  $\sim 3.5$  h. J2253+1608 was observed as fringe finder, and was also used to calibrate the bandpass.

We performed standard a priori gain calibration within *AIPS*, using the measured gains and system temperatures of each antenna. We fringe-fit and imaged the data for the calibrator J2333+3901 in a standard manner. The final image for J2333+3901 was then included as an input image in a new round of fringe-fitting for J2333+3901. In this way, the results obtained for the phase delays and delay-rates for J2333+3901 were structure-free. These new values were then interpolated and applied to B3 J2330+3927 using *AIPS* standard procedures. These technicalities allowed us to estimate the positions of components inside B3 J2330+3927 with milliarcsecond astrometric precision (see Table 1).

To properly image the arcsecond-wide source B3 J2330+3927 with milliarcsecond resolution, we kept

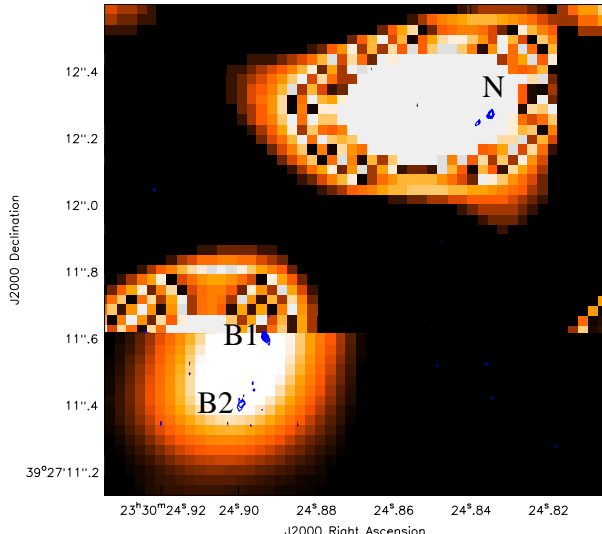


**Figure 2.** Central part of the VLA 8.4 GHz image showing components N and B with the VLBA 1.7 GHz image overlaid as blue contours. Contour levels are a geometric progression in  $\sqrt{2}$ , with the first contour starting at  $0.36 \text{ mJy beam}^{-1}$ .

the averaging integration time to 2 s and used a maximum channel bandwidth in the imaging process of 2 MHz at each frequency, which results in a maximum degradation of the peak response for the component furthest away from the phase center of less than  $\sim 4\%$  and prevents artificial smearing of the images (e.g., Bridle & Schwab 1999). We used standard phase self-calibration techniques within AIPS to image B3 J2330+3927 at both frequencies. The image off-source rms was  $\sim 60 \mu\text{Jy}$  at both 1.7 and 5.0 GHz.

#### 4 RESULTS AND DISCUSSION

Figure 1 shows the reanalyzed 8.4 GHz VLA data on B3 J2330+3927, with the archival 1.4 GHz data overlaid. In addition to the three components identified by DB03, we also detect a faint component on the northwestern side of object *a*. In the following, we call these components A, B, C, and N, as identified in Fig. 1 and Table 1. The newly found component A, shows for the first time the detection of the counter-jet in B3 J2330+3927, providing support for the interpretation that the radio component N, coincident with object *a*, is the radio core.

We used the VLBA to image with mas-resolution the entire VLA region, encompassing objects A through C. We detected components N and B only, both at 1.7 and 5.0 GHz. Figure 2 shows the 8.4 GHz map of these components, with the 1.7 GHz VLBA map overlaid. Figure 3 displays blow-outs of components N and B to show the VLBA data at their full resolution. Our 1.7 GHz VLBA data shows that region N consists of a strong source N1, composed of a very compact region and a protrusion which likely corresponds to the jet, and a relatively faint, jet-like feature, N2, at a position angle of  $\approx 125^\circ$ . Component B also splits into two components, B1 and B2, at a position angle of  $\approx 160^\circ$ . Component B1 shows an elongated structure at a position angle of  $\approx 132^\circ$ , thus forming an angle of  $68^\circ$  with respect to the

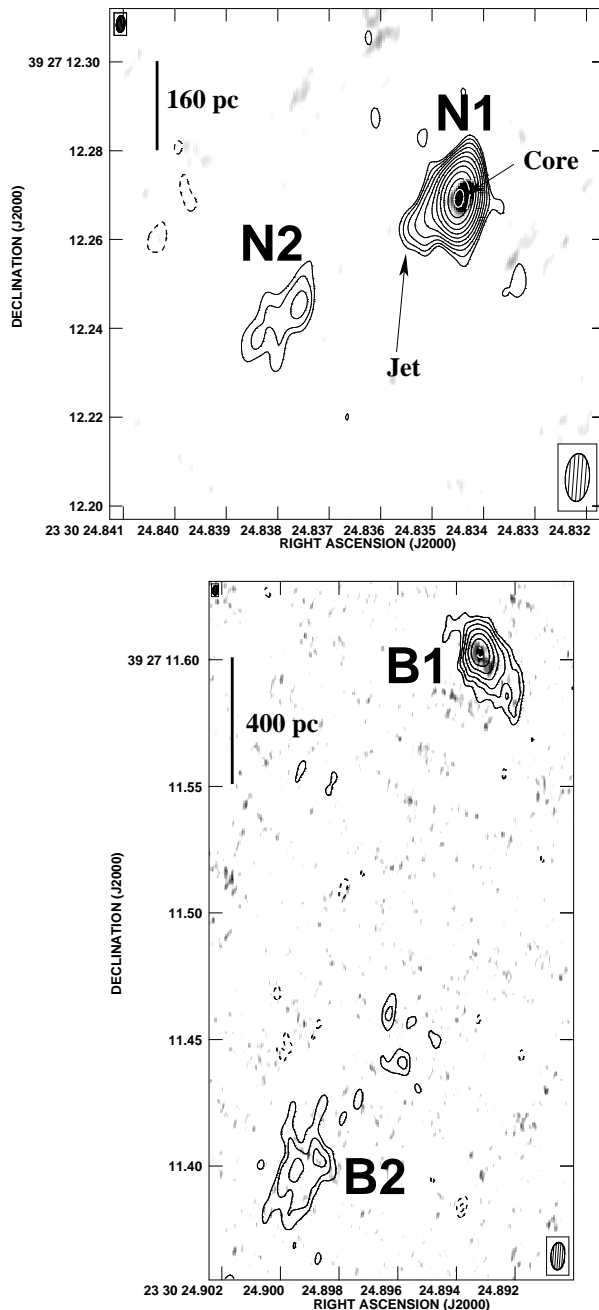


**Figure 3.** VLBA 5.0 GHz images of components N (top) and B (bottom) shown in greyscales with VLBA 1.7 GHz contours overlaid. Contour levels are a geometric progression in  $\sqrt{2}$ , with the first contour starting at  $0.1 \text{ mJy beam}^{-1}$ . Note the protrusion southeast of component N1, which corresponds to the jet emanating from the radio core, as confirmed by the detection of N2. Note that the jet bends by  $\approx 35^\circ$  between N2 and B1 (see text), and that B1 is extended perpendicular to the jet axis.

line connecting B1 and B2. Our 5.0 GHz VLBA data only detect components N1 and B1. Table 1 lists the flux densities and positions for all these VLBA and VLA components. Component N1 has a spectral index  $\alpha_{5.0}^{1.7} = -0.2 \pm 0.1$  and B1 has  $\alpha_{5.0}^{1.7} = -1.2 \pm 0.1$ , while components N2 and B2 both have  $\alpha_{5.0}^{1.7} \lesssim -0.9$ . Because component N1 has the flat-

**Table 1.** Gaussian component fits of B3 J2330+3927.

$\nu$ GHz	Comp. Name	$\Delta\text{RA}$ J2000	$\Delta\text{DEC}$ J2000	$S_{\text{peak}}$ mJy/beam	$S_{\text{tot}}$ mJy
1.7 <sup>†</sup>	N1	24 <sup>h</sup> 8345	12 <sup>h</sup> 269	10.45	$13.47 \pm 0.68$
	N2	24 <sup>h</sup> 8381	12 <sup>h</sup> 242	0.71	$1.89 \pm 0.11$
	B1	24 <sup>h</sup> 8932	11 <sup>h</sup> 603	2.45	$9.89 \pm 0.50$
	B2	24 <sup>h</sup> 8997	11 <sup>h</sup> 397	0.71	$5.53 \pm 0.28$
5.0 <sup>†</sup>	N1	24 <sup>h</sup> 8345	12 <sup>h</sup> 269	6.70	$11.38 \pm 0.57$
	B1	24 <sup>h</sup> 8932	11 <sup>h</sup> 602	0.35	$2.77 \pm 0.15$
8.4 <sup>‡</sup>	A	24 <sup>h</sup> 780	13 <sup>h</sup> 12	0.31	$0.35 \pm 0.05$
	N	24 <sup>h</sup> 837	12 <sup>h</sup> 31	10.02	$10.80 \pm 0.54$
	B	24 <sup>h</sup> 900	11 <sup>h</sup> 53	3.74	$6.28 \pm 0.31$
	C	24 <sup>h</sup> 923	10 <sup>h</sup> 63	2.55	$3.98 \pm 0.18$

The component names are marked in Figs. 1, 2, and 3; the reference coordinates are 23<sup>h</sup>30<sup>m</sup>0<sup>s</sup>0 for RA, and 39<sup>°</sup>27'0"0 for DEC. The standard errors in the quoted VLBA positions are  $\approx 1$  mas in each coordinate, while those for the VLA positions are estimated to be  $\approx 30$  mas. The standard errors in the flux density estimates are the result of adding in quadrature the image off-source rms and a 5% of the peak flux density at each frequency, to account for inaccuracies of the system calibration. <sup>†</sup> From VLBA observations at 1.7 and 5.0 GHz. <sup>‡</sup> From VLA observations at 8.4 GHz.

test spectral index of all components and is very compact, we identify it with the radio core of B3 J2330+3927, which is located at the position of the optical/near-IR type II AGN and the peak of the CO(4-3) emission (DB03). We note that the extrapolated VLBA flux density at 8.4 GHz for N1 ( $\approx 10.8$  mJy) is very close to the observed VLA flux, implying that most of the VLA emission comes from the core. Indeed, the fraction of the 8.4 GHz core emission,  $f_c \approx 0.50$ , is extremely large for a radio galaxy, and even large for quasar standards (Saikia et al. 1995). The extrapolated VLBA flux density from component B1 at 8.4 GHz is  $\approx 1.5$  mJy, substantially lower than observed, indicating that a significant amount of flux density comes from a rather extended region.

With the new information yielded by our VLBA observations, we can now describe a consistent picture of the radio structure of B3 J2330+3927: the source radio emission is core-dominated, and its morphology very asymmetric, with a lobe distance ratio  $Q = (N1 - C)/(N1 - A) \approx 1.93$  (see Table 1), and a lobe flux density ratio  $R = S_C/S_A \gtrsim 11$  (from the 8.4 GHz VLA observations). We can exclude significant radio emission beyond component A, because our wide-field 1.4 GHz VLA map ( $1^{\circ} \times 1^{\circ}$ ) is very deep, and no other components are seen in the WENSS (Rengelink et al. 1997) or NVSS (Condon et al. 1998). The change in position angle between the jet-like feature emanating from the core, N1-jet and N2, and the line connecting components B1 and B2, indicates that the radio jet is deflected between components N and B. Jet bending can be naturally explained by the interaction of the jet with its ambient medium (e.g., Saxton et al. 2005) or, alternatively, as the precession of the jet in a binary black hole system (e.g., Hummel et al. 1988). Interestingly, no increase in the Ly- $\alpha$  emission is seen in the 2D spectrum (Fig. 4 of DB03), in contrast to similarly deflected radio jets in other HzRGs, showing bright Ly- $\alpha$  emission at these bendings (e.g. van Ojik et al. 1996).

The values of  $R$  and  $Q$  obtained for B3 J2330+3927 are more common of quasars than radio galaxies, although statistical analyses by McCarthy et al. (1991) did

not show these differences to be highly significant. However, Best et al. (1995) show convincing evidence that quasars have more asymmetric radio morphologies than radio galaxies. This finding is consistent with one of the prime expectations of the unified model, namely that quasars and radio galaxies are intrinsically similar, but quasars are observed when the radio jet axis of the source is within 45<sup>°</sup> of the line of sight (Barthel 1989). In addition, quasars also display larger  $f_c$  values than radio galaxies (Saikia et al. 1995). Therefore, based on its radio morphology, B3 J2330+3927 would be classified as a type I AGN. However, the optical and near-IR Keck spectra (Fig. 5 of DB03) clearly show only narrow emission lines with relatively strong HeII  $\lambda 1640$  and very faint H $\beta$  typical of type II AGN. Moreover, the optical and near-IR continuum emission is weak ( $F[\lambda_{\text{rest}} = 1500\text{\AA}] \approx 5 \times 10^{-19} \text{ erg s}^{-1} \text{ cm}^{-2} \text{\AA}^{-1}$ ) and relatively red ( $F_{\lambda} \propto \lambda^{2.7}$ ), as is common in type II AGN.

We now examine three possibilities to explain the observed asymmetries of the radio structure of B3 J2330+3927: (i) environmental effects, (ii) relativistic beaming effects, and (iii) intrinsic asymmetries. To date, almost all cases of asymmetry in radio galaxies have been explained by environmental effects. In the most detailed study to date, McCarthy et al. (1991) find that for radio-loud type II AGN, the radio lobe closest to the core always lies on the same side of the nucleus as the high surface brightness optical line emission. This is contrary to what is seen in B3 J2330+3927. Fig. 4 of DB03 shows that the Ly- $\alpha$  emission extends from the radio core N to the southern radio lobe C, which is almost twice further away from the core than the faint radio lobe A. One could argue that the Ly- $\alpha$  emission towards lobe A is quenched by dust, which is revealed by its strong far-IR emission (Stevens et al. 2003, DB03). However, the spatial profiles of the non-resonant [OII]  $\lambda 3727$  and [OIII]  $\lambda 5007$  lines in the Keck/NIRC spectra of DB03 show a similar shape, with no emission towards lobe A, indicating that no substantial emission line flux is missing in the Ly- $\alpha$  profile. Environmental effects thus do not seem to play a major role in the radio morphology of B3 J2330+3927.

Turning to relativistic beaming effects, we note that jet speed,  $\beta$ , viewing angle,  $\phi$ , and arm-length ratio,  $Q$ , are related by  $\beta \cos \phi = (Q - 1)/(Q + 1)$  (e.g., Best et al. 1995). The fact that we observe a clear type II AGN indicates that the viewing angle with respect to the line of sight should be  $\phi > 45^{\circ}$ . However, the fraction of the emission from the nuclear component,  $f_c = 0.50$  at 8.4 GHz, is very large for a radio galaxy, and suggests the viewing angle must be then close to the  $\phi = 45^{\circ}$  limit. If this is the case, the obtained arm-length ratio  $Q \approx 1.9$  requires then a jet speed of  $\beta \approx 0.45$ . Now, the observed ratio of the flux densities of components C and A is  $R \gtrsim 11$ . If components A and C are optically-thin, isotropically emitting jets, their flux ratio should then be, within the relativistic beaming scenario (e.g., Mirabel & Rodríguez 1999 and references therein), equal to  $(\frac{1+\beta \cos \theta}{1-\beta \cos \theta})^{k-\alpha}$ , where  $k=2$  for a continuous jet, and  $k=3$  for the case of discrete condensations. Assuming that components A and C have a spectral index of  $\alpha = -0.9$ , the flux ratio for a continuous jet would be  $\lesssim 4$ , whereas for discrete condensations would be  $\lesssim 6$ . Our observed value of  $R \gtrsim 11$  is therefore difficult to explain within the standard relativistic beaming framework.

The most likely explanation of the observed asymmetry thus seems to be an intrinsic difference in the radio jets. Examples of such radio galaxies are very rare in the literature, and have only been reported at low redshifts, for example in the  $z=0.290$  radio galaxy 4C 63.07 (Saikia et al. 1996). Sources like B3 J2330+3927 and 4C 63.07 are difficult to reconcile with predictions from the standard unified model for quasars and radio galaxies (Barthel 1989).

We estimated the energetics and magnetic fields in the regions N and B of B3 J2330+3927, using our VLBA images. We measured the angular sizes of components N1 and B1, and used their flux densities and spectral indices between 1.7 and 5.0 GHz to characterize them using standard prescriptions (e.g., Miley 1980). We assumed spectral cut-off frequencies of  $\nu_1=0.01$  GHz and  $\nu_2=100$  GHz, a ratio of heavy particles to electrons  $k=100$ , and a filling factor of the emitting regions of 1. N1, the core, is characterized by a synchrotron radio luminosity of  $L_R \sim 3 \times 10^{45}$  erg s $^{-1}$ , an average magnetic field  $B \sim 7$  mG, a minimum energy density  $u_{\text{me}} \sim 5 \times 10^{-6}$  erg cm $^{-3}$ , and a (minimum) total energy  $E_{\text{tot}} \sim 7 \times 10^{56}$  erg. The radio region B1 displays similar values:  $B \sim 14$  mG,  $u_{\text{rel}} \sim 2 \times 10^{-5}$  erg cm $^{-3}$ ,  $E_{\text{tot}} \sim 8 \times 10^{57}$  erg,  $L_R \sim 8 \times 10^{44}$  erg s $^{-1}$ . Our estimates of the magnetic field in those components are in good agreement with magnetic field estimates for other HzRGs (e.g., Cai et al. 2002), and significantly higher than estimates found in typical nearby powerful radio galaxies (e.g.,  $B \sim 3 \times 10^{-4}$  for Cygnus A; Carilli & Barthel 1996). If there is no energy resupply to the above radio source components, a radiative source component lifetime can be estimated as  $\tau = E_{\text{rel}}/L_R$ , where  $E_{\text{rel}} = 7/4(1+k)^{-1}E_{\text{tot}}$  (Pacholczyk 1970). This leads to  $\tau \sim 2 \times 10^4$  yr and  $\tau \sim 7 \times 10^5$  yr for N1 and B1, respectively. Since the average age of the relativistic electrons,  $t_r$ , in N1 and B1 is in both cases  $\sim 600$  yr, i.e.,  $t_r \ll \tau$ , it follows that a continuous supply of newly accelerated electrons is required to explain the observed radio emission in those regions.

## 5 SUMMARY

The main results of our VLBA and VLA analysis of B3 J2330+3927 can be summarized as follows:

(i) We identify component N1, a rather compact, flat spectrum ( $\alpha \approx -0.2$ ) with the core. It is located at the position of the optical/near-IR type II AGN and the peak of the CO(4-3) emission.

(ii) The 1.4 and 8.4 GHz VLA images reveal a previously undetected, very faint counterjet. The 8.4 GHz VLA image shows that B3 J2330+3927 has a radio lobe flux density ratio  $R \gtrsim 11$ , a radio lobe asymmetry ratio  $Q \approx 1.9$ , and a fraction of core emission  $f_c \approx 0.50$ . These values are much more compatible to quasars, and not expected to occur in radio galaxies. However, B3 J2330+3927 is a bona-fide type II AGN by virtue of its optical and near-IR spectra.

(iii) The fact that almost all the Ly- $\alpha$  emission is located at the side where the radio lobe is further away from the core is contrary to what has been observed in other radio galaxies. This argues against environmental effects as the origin of the radio source asymmetry. Relativistic beaming effects also cannot explain the observed flux density asymmetry, implying an intrinsic asymmetry of the radio jets.

This is the first example of such a source at high redshift, and seems to be difficult to reconcile with the unified model.

(iv) We estimated the energetics and magnetic field of the innermost regions of B3 J2330+3927. We find values of the order of  $B \sim 7-15$  mG for N1 and B1, values that are significantly higher than estimates found in typical nearby powerful radio galaxies (e.g.,  $B \sim 0.3$  mG for Cygnus A). From the estimated radiative lifetimes for those regions, we conclude that a continuous supply of newly accelerated electrons is required to explain the observed radio emission.

## ACKNOWLEDGMENTS

We thank R. Ivison for providing the calibrated 1.4 GHz VLA data, R. Laing for stimulating discussions, and an anonymous referee for a prompt and useful report. This research has been partially funded by grant AYA2001-2147-C02-01 of the Spanish Ministerio de Ciencia y Tecnología. MAPT is supported by the programme Ramón y Cajal of the Spanish Ministerio de Educación y Ciencia. NRAO is a facility of the National Science Foundation operated under cooperative agreement by Associated Universities, Inc. This research has made use of NASA's ADS.

## REFERENCES

- Barthel P. 1989, ApJ, 336, 606
- Best P., Bailer D., Longair M., & Riley J. 1995, MNRAS, 275, 1171
- Bicknell G., et al. 2000, ApJ, 540, 678
- Blundell K., & Rawlings S. 1999, Nature, 399, 330
- Bridle A., Schwab F. 1999, ASP Conf. Ser. 180: Synthesis Imaging in Radio Astronomy II, 180, 371
- Cai Z., et al. 2002, A&A, 381, 401
- Carilli C. & Barthel P. 1996, Astron. Astroph. Rev., 7, 1
- Carilli C., et al. 2002, ApJ, 567, 781
- Chambers K., Miley G. & van Breugel W. 1987, Nature, 329, 604
- Condon J., et al. 1998, AJ, 115, 1693
- De Breuck C., van Breugel W., Stanford S. A., Röttgering H., Miley G. & Stern D. 2002 AJ, 123, 637
- De Breuck C., et al. 2003, A&A, 401, 911
- Hummel C.A., et al. 1988, A&A, 257, 489
- McCarthy P., van Breugel W. & Kapahi V. 1991, ApJ, 371, 478
- Mirabel I.F. & Rodríguez L.F. 1999, ARA&A, 37, 409
- Miley G. 1980, ARA&A, 18, 165
- Overzier R.A., Harris D.E., Carilli C.L., Pentericci L., Röttgering H.J.A., Miley G.K. 2005, A&A, 433, 87
- Pacholczyk A. 1970, Radio Astrophysics (San Francisco: Freeman)
- Rengelink, R. et al. 1997, A&A, 124, 259
- Rocca-Volmerange B., Le Borgne D., De Breuck C., Fioc M. & Moy, E. 2004, A&A, 415, 931
- Saikia D. J., Jeyakumar S., Wiita P. J., Sanghera H. S. & Spencer R.E. 1995, MNRAS, 276, 1215
- Saikia D. J., Thomasson P., Jackson N., Salter C., & Junor W. 1996, MNRAS, 282, 837
- Saxton C., Bicknell G., Sutherland R., & Midgley S. 2005, MNRAS, 359, 781

Scharf C., et al. 2003, ApJ, 596, 105  
Stevens J., et al. 2003, Nature, 425, 264  
Venemans B.P., et al. 2004, A&A, 424, L17  
van Ojik R., Röttgering H., Carilli C., Miley G., Bremer,  
& Macchetto D. 1996, A&A, 313, 25